Changes in the Cation Ordering of Layered O3 $Li_xNi_{0.5}Mn_{0.5}O_2$ during Electrochemical Cycling to High Voltages: An Electron Diffraction Study

Hayley H. Li,[†] Naoaki Yabuuchi,[†] Ying S. Meng,[‡] Sundeep Kumar,[†] Julien Breger,[§] Clare P. Grey,[§] and Yang Shao-Horn*,[†]

Department of Mechanical Engineering and Department of Materials Science and Engineering, Massachusetts Institute of Technology, Cambridge, Massachusetts 02139, and SUNY Stony Brook, Stony Brook, New York 11794

Received January 15, 2007. Revised Manuscript Received March 10, 2007

Selected area electron diffraction patterns were collected from pristine $LiNi_{0.5}Mn_{0.5}O_2$ and cycled $Li_xNi_{0.5}Mn_{0.5}O_2$ samples (to either 4.5 V or 5.3 V) in the charged and discharged states. Superlattice reflections characteristic of the $\sqrt{3}a_{Hex.} \times \sqrt{3}a_{Hex.} \times c_{Hex.}$ supercell, which are associated with ordering of Li-rich and Li-deficient sites in the transition metal layer of the pristine sample, were weakened considerably or disappeared completely in the charged samples, indicating a reduction of this long-range ordering. Detailed analysis revealed not only a considerable amount of Ni migration from the Li layer to the transition metal layer upon charging to 4.5 V but also that a complete removal of Ni from the Li layer might be possible upon charging to 5.3 V as evidenced by the detection of the O1 phase with a hexagonal-close-packed oxygen array. The Ni migration was in part reversible upon discharge as the fractions of crystals exhibiting the $\sqrt{3}a_{Hex.} \times \sqrt{3}a_{Hex.} \times c_{Hex.}$ superlattice reflections were considerably higher in the discharged samples than in the charged samples. Additional superlattice reflections that could not be indexed to the $\sqrt{3}a_{Hex.} \times \sqrt{3}a_{Hex.} \times c_{Hex.}$ supercell were observed in some crystallites of the cycled samples, the extent of ordering varying from crystal to crystal. This new long-range ordering was attributed to a nonrandom distribution of Li, Ni, and vacancies in the tetrahedral and/or octahedral sites of the Li layer. Although the nature of this long-range ordering is not fully understood, it is proposed that the Li, Ni, and vacancies order on the tetrahedral sites of the Li layer resulting in a $2a_{Hex.} \times 2a_{Hex.} \times c_{Hex.}$ supercell with space group $R\bar{3}m$, in the charged samples, while they order on the tetrahedral and octahedral sites of the Li layer in an $a_{Mon.} \times a_{Mon.} \times c_{Mon.}$ cell having space group $P2/m$, in the discharged samples. The appearance of long-range ordering in the Li layer of the cycled samples is likely due to electrostatic repulsion of cations, which might play an important role in the stability of the O3 layered structure and lithium diffusion in the layered structure.

Introduction

$LiNi_{0.5}Mn_{0.5}O_2$ has been studied widely as a positive electrode material for high-energy and high-power advanced lithium-ion batteries.[1−15] First-principles[6,7,13] and X-ray absorption near-edge structure (XANES) studies[8−11] have shown that the Ni ions are 2+ ($t_{2g}^6 e_g^2$) and the Mn ions are 4+ (t_{2g}^3) in $LiNi_{0.5}Mn_{0.5}O_2$, instead of 3+ in $LiNiO_2$ ($t_{2g}^6 e_g^1$) and $LiMnO_2$ ($t_{2g}^3 e_g^1$). Typically, ∼0.10 Li^+ per formula unit is found in the transition metal layer of the O3 layered $LiNi_{0.5}Mn_{0.5}O_2$ structure, which displaces an equivalent amount of Ni^{2+} to the Li layer. Previous computational studies have shown that reducing the size difference between Li and transition metal ions increases cation disorder or interlayer mixing.[16] In the short-range, Li ions in the transition metal layer are preferentially surrounded by Mn ions as revealed by NMR studies.[10] Disorder or mixing of

* To whom correspondence should be addressed. E-mail: shaohorn@mit.edu.
[†] Department of Mechanical Engineering, Massachusetts Institute of Technology.
[‡] Department of Materials Science and Engineering, Massachusetts Institute of Technology.
[§] SUNY Stony Brook.

(1) Ohzuku, T.; Makimura, Y. *Chem. Lett.* **2001**, *30*, 744.
(2) Lu, Z. H.; MacNeil, D. D.; Dahn, J. R. *Electrochem. Solid State Lett.* **2001**, *4*, A191.
(3) Ohzuku, T.; Ariyoshi, M.; Makimura, Y.; Yabuuchi, N.; Sawai, K. *Electrochemistry* **2005**, *73*, 2.
(4) Lu, Z. H.; Beaulieu, L. Y.; Donaberger, R. A.; Thomas, C. L.; Dahn, J. R. *J. Electrochem. Soc.* **2002**, *149*, A778.
(5) Makimura, Y.; Ohzuku, T. *J. Power Sources* **2003**, *119*, 156.
(6) Koyama, Y.; Makimura, Y.; Tanaka, I.; Adachi, H.; Ohzuku, T. *J. Electrochem. Soc.* **2004**, *151*, A1499.
(7) Reed, J.; Ceder, G. *Electrochem. Solid State Lett.* **2002**, *5*, A145.
(8) Kobayashi, H.; Sakaebe, H.; Kageyama, H.; Tatsumi, K.; Arachi, Y.; Kamiyama, T. *J. Mater. Chem.* **2003**, *13*, 590.
(9) Makimura, Y. Ph.D. Thesis, Osaka City University, 2003.
(10) Yoon, W. S.; Paik, Y.; Yang, X. Q.; Balasubramanian, M.; McBreen, J.; Grey, C. P. *Electrochem. Solid State Lett.* **2002**, *5*, A263.
(11) Nakano, H.; Nonaka, T.; Okuda, C.; Ukyo, Y. *J. Ceram. Soc. Jpn.* **2003**, *111*, 33.
(12) Arachi, Y.; Kobayashi, H.; Emura, S.; Nakata, Y.; Tanaka, M.; Asai, T.; Sakaebe, H.; Tatsumi, K.; Kageyama, H. *Solid State Ionics* **2005**, *176*, 895.
(13) Van der Ven, A.; Ceder, G. *Electrochem. Commun.* **2004**, *6*, 1045.
(14) Johnson, C. S.; Kim, J. S.; Kropf, A. J.; Kahaian, A. J.; Vaughey, J. T.; Fransson, L. M. L.; Edstrom, K.; Thackeray, M. M. *Chem. Mater.* **2003**, *15*, 2313.
(15) Kang, K. S.; Meng, Y. S.; Breger, J.; Grey, C. P.; Ceder, G. *Science* **2006**, *311*, 977.
(16) Wu, E. J.; Tepesch, P. D.; Ceder, G. *Philos. Mag. B* **1998**, *77*, 1039.

10.1021/cm070139+ CCC: $37.00 © 2007 American Chemical Society
Published on Web 04/20/2007

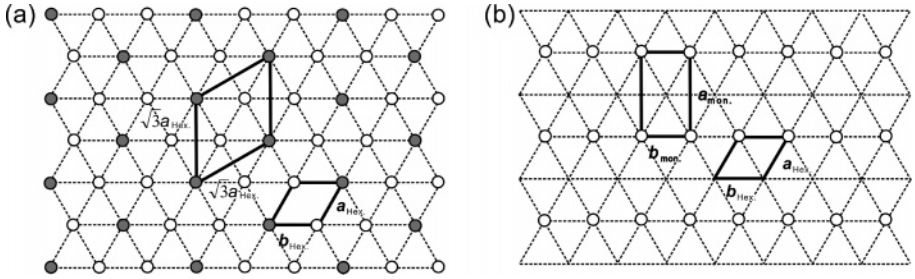

Figure 1. (a) $\sqrt{3}a_{Hex.} \times \sqrt{3}a_{Hex.} \times c_{Hex.}$ supercell present in the pristine $LiNi_{0.5}Mn_{0.5}O_2$ sample with in-plane ordering of Li-rich and Li-deficient sites in a ratio of 1:2 in the trigonal lattice. (b) Schematic of octahedral site ordering under the *P*2/*m* symmetry.

Li^+ and Ni^{2+} in alternative layers may result from the fact that they have similar ionic radii[17] (Li^+, 0.76 Å, and Ni^{2+}, 0.69 Å) and the strong driving force for Li^+/Mn^{4+} ordering. Previous electron diffraction studies have revealed long-range cation ordering resulting in a $\sqrt{3}a_{Hex.} \times \sqrt{3}a_{Hex.} \times c_{Hex.}$ supercell with space group $P3_112$.[18,19] This type of ordering creates two different crystallographic sites, one that is Li-rich and one that is Li-deficient (Figure 1a) and is analogous to that reported in Li_2MnO_3,[20] $Li_{0.33}CoO_2$,[21,22] and $Li_{0.33}NiO_2$.[23] Cation occupancies of each site can be clearly defined[24] in these latter structures, which have a long-range order parameter of unity.[25] However, partial occupancy of Li^+, Mn^{4+}, and Ni^{2+} on the two different sites in $LiNi_{0.5}Mn_{0.5}O_2$ prevents a precise determination of the exact occupancy for each site, as discussed previously.[18,19] Although the presence of Ni in the Li layer is believed generally to have detrimental effects in the reversibility of lithium intercalation and the de-intercalation process by impeding Li diffusion in the Li slab space, $Li/LiNi_{0.5}Mn_{0.5}O_2$ cells have shown excellent reversible capacities.[1,2,4,5] This is in contrast to the reversibility found for $Li/Li_{1-z}Ni_{1+z}O_2$ cells,[26] which is very sensitive to extra Ni (*z* value) in the Li layer. The apparent difference might be related to how the structures of $Li_xNi_{0.5}Mn_{0.5}O_2$ and $Li_{1-z-x}Ni_{1+z}O_2$ change upon lithium removal and electrochemical cycling.

Recent diffraction and NMR data reveal that the arrangement of cations in the layered structure changes considerably upon lithium removal from $LiNi_{0.5}Mn_{0.5}O_2$. ^6Li magic angle spinning (MAS) NMR studies and first-principles studies[10,27,28] have revealed that the Li ions in the transition metal layer are electrochemically active and have shown that the ~3.9 V voltage plateau on the first charge is associated with the simultaneous removal of Li ions from the Li and transition metal layers (Figure 2). It has been reported that Li ions can migrate and fill tetrahedral sites adjacent to vacant Li octahedral sites in the transition metal layer at the beginning of charge,[28] which can then be removed toward the end of charge at high voltages[13] above 5 V versus Li/Li^+. Li migration into the tetrahedral sites in the Li layer was first suggested from Rietveld refinement of synchrotron powder X-ray diffraction data[12,29] of charged $Li_xNi_{0.5}Mn_{0.5}O_2$ samples. The presence of Li on the tetrahedral sites has been confirmed recently by neutron diffraction measurements,[27] where ~0.10 Li per formula unit has been detected in the tetrahedral sites in the $Li_xNi_{0.5}Mn_{0.5}O_2$ samples ($x = 0.62$ and 0.33). In addition, synchrotron X-ray data have detected some Ni ions (~0.01 per formula unit) in the tetrahedral sites of the Li layer in $Li_{0.5}Ni_{0.5}Mn_{0.5}O_2$, having the tetrahedral site occupancy increasing upon further lithium removal.[12,29] Li^+ and Ni^{2+} ions in the Li layer that share an edge with the vacant octahedron in the transition metal layer left behind by the de-intercalated Li^+ may hop into the face-shared tetrahedral sites,[27,28] as shown in Figure 2. Such migration is highly unfavorable in layered Li_xCoO_2 and $Li_{1-z-x}Ni_{1+z}O_2$ as no vacancies are present in the transition metal layer, and tetrahedral and adjacent face-sharing octahedral sites cannot be occupied simultaneously because of the small interatomic distance and large electrostatic repulsion between cations. Moreover, recent neutron powder diffraction data have indicated that Ni ions can migrate from the Li layer to the transition metal layer upon charging to high voltages.[27] As indicated from these aforementioned reports, structural changes in $Li_xNi_{0.5}Mn_{0.5}O_2$ upon lithium removal and electrochemical cycling are more complex and quite different from those found in other layered Li_xCoO_2[30−32] and $Li_{1-z-x}Ni_{1+z}O_2$.[33−37]

(17) Shannon, R. D. *Acta Crystallogr., Sect. A* **1976**, *32*, 751.
(18) Meng, Y. S.; Ceder, G.; Grey, C. P.; Yoon, W. S.; Jiang, M.; Breger, J.; Shao-Horn, Y. *Chem. Mater.* **2005**, *17*, 2386.
(19) Meng, Y. S.; Ceder, G.; Grey, C. P.; Yoon, W. S.; Shao-Horn, Y. *Electrochem. Solid State Lett.* **2004**, *7*, A155.
(20) Strobel, P.; Lambertandron, B. *J. Solid State Chem.* **1988**, *75*, 90.
(21) Van der Ven, A.; Aydinol, M. K.; Ceder, G.; Kresse, G.; Hafner, J. *Phys. Rev. B* **1998**, *58*, 2975.
(22) Shao-Horn, Y.; Levasseur, S.; Weill, F.; Delmas, C. *J. Electrochem. Soc.* **2003**, *150*, A366.
(23) Delmas, C.; Menetrier, M.; Croguennec, L.; Levasseur, S.; Peres, J. P.; Pouillerie, C.; Prado, G.; Fournes, L.; Weill, F. *Int. J. Inorg. Mater.* **1999**, *1*, 11.
(24) Cowley, J. M. *Diffraction Physics*, 3 ed.; North Holland: Amsterdam, 1995.
(25) Warren, B. E. *X-Ray Diffraction*; Dover Publications: New York, 1990.
(26) Peres, J. P.; Delmas, C.; Rougier, A.; Broussely, M.; Perton, F.; Biensan, P.; Willmann, P. *J. Phys. Chem. Solids* **1996**, *57*, 1057.
(27) Breger, J.; Meng, Y. S.; Hinuma, Y.; Kumar, S.; Kang, K.; Shao-Horn, Y.; Ceder, G.; Grey, C. P. *Chem. Mater.* **2006**, *18*, 4768.
(28) Grey, C. P.; Yoon, W. S.; Reed, J.; Ceder, G. *Electrochem. Solid State Lett.* **2004**, *7*, A290.
(29) Kobayashi, H.; Arachi, Y.; Kageyama, H.; Tatsumi, K. *J. Mater. Chem.* **2004**, *14*, 40.
(30) Ohzuku, T.; Ueda, A. *J. Electrochem. Soc.* **1994**, *141*, 2972.
(31) Reimers, J. N.; Dahn, J. R. *J. Electrochem. Soc.* **1992**, *139*, 2091.
(32) Amatucci, G. G.; Tarascon, J. M.; Klein, L. C. *J. Electrochem. Soc.* **1996**, *143*, 1114.
(33) Ohzuku, T.; Ueda, A.; Nagayama, M. *J. Electrochem. Soc.* **1993**, *140*, 1862.
(34) Li, W.; Reimers, J. N.; Dahn, J. R. *Solid State Ionics* **1993**, *67*, 123.
(35) Arai, H.; Okada, S.; Ohtsuka, H.; Ichimura, M.; Yamaki, J. *Solid State Ionics* **1995**, *80*, 261.
(36) Pouillerie, C.; Suard, E.; Delmas, C. *J. Solid State Chem.* **2001**, *158*, 187.
(37) Croguennec, L.; Pouillerie, C.; Mansour, A. N.; Delmas, C. *J. Mater. Chem.* **2001**, *11*, 131.

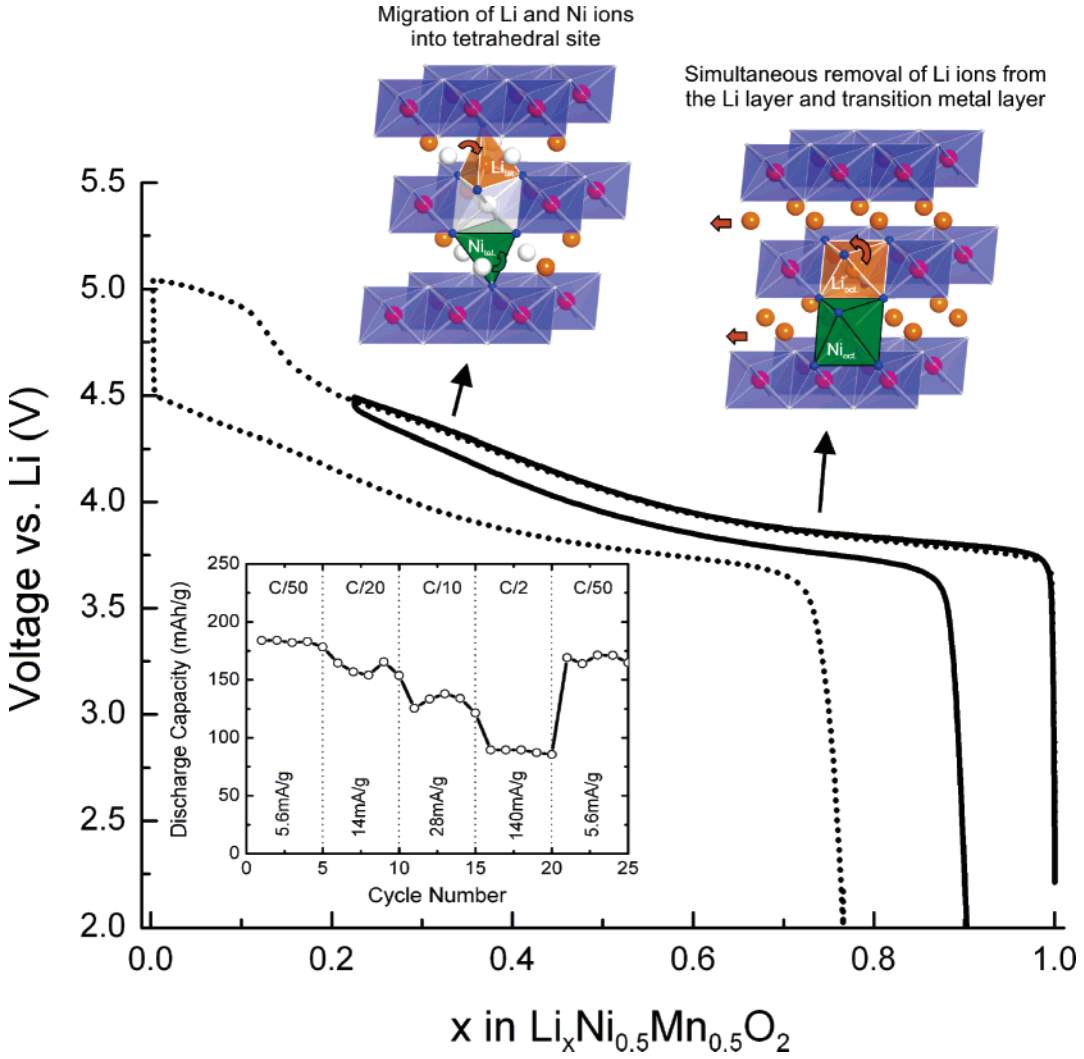

Figure 2. Representative galvanostatic charge and discharge voltage profile of Li/$Li_xNi_{0.5}Mn_{0.5}O_2$ cells under a current density of *C*/50 (0.027 mA/cm^2) in the voltage ranges of 2.0−4.5 V (solid line) and 5.1 V (dotted line) and schematics of $Li_xNi_{0.5}Mn_{0.5}O_2$ structure showing reported processes of Li and Ni motion at different Li contents. At the beginning of charge, Li ions are simultaneously removed from the Li and transition metal layers. Upon further de-intercalation of Li ions, Li and Ni ions can migrate into the tetrahedral sites that share a face with vacant octahedral sites in the transition metal layer. The inset shows the discharge capacities for the first 25 cycles collected at various current densities in the voltage range of 2.5 and 4.5 V, where no significant loss in the capacity is noted upon cycling.

Changes in the cation arrangement and ordering can play a significant role in the electrochemical properties and stability of cycled $Li_xNi_{0.5}Mn_{0.5}O_2$. Electron diffraction is more sensitive to cation ordering in comparison to X-ray and neutron powder diffraction. Recent single-crystal electron diffraction analyses have clearly revealed superlattice reflections associated with lithium and vacancy ordering in the octahedral sites of O3 layered $Li_{0.5}CoO_2$[22] and Li_xNiO_2,[23,38] while these superlattice reflections are either not visible or extremely weak in the powder diffraction data. Arachi et al.[12,39] have proposed cation ordering in the monoclinic phase found for the $Li_xNi_{0.5}Mn_{0.5}O_2$ ($0.33 \leq x \leq 0.7$) sample. The in-plane dimensions of this monoclinic cell are outlined in Figure 1b, which shows its relationship to the present hexagonal cell ($a_{Mon.} = \sim\sqrt{3}a_{Hex.}$ and $b_{Mon.} = \sim b_{Hex.}$). However, no details on the nature of cation ordering are discussed, and the space group *C*2/*m* of the monoclinic cell used in these studies[12,29] describes only a structural distortion, with cations in the octahedral and tetrahedral sites randomly distributed in the Li and transition metal layer.

The focus of this study is to investigate how cation arrangements and ordering change in $Li_xNi_{0.5}Mn_{0.5}O_2$ samples in the charged and discharged states, by using selected area electron diffraction. Li removal from the transition metal layer and Ni migration might change the extent of cation ordering in the $\sqrt{3}a_{Hex.} \times \sqrt{3}a_{Hex.} \times c_{Hex.}$ supercell found in the pristine $LiNi_{0.5}Mn_{0.5}O_2$. In addition, as Li and Ni ions can reside in octahedral and tetrahedral sites of the Li layer, ordering in these octahedral and tetrahedral sites might be possible because of electrostatic forces among cations. Figure 3 shows tetrahedral 6c sites of the Li layer in the O3 layered structure having a cubic closed-packed oxygen array (AB CA BC...). There are two tetrahedral sites per octahedral site in the Li layer (one pointing up and the other pointing down), which share face with adjacent octahedral sites in the transition metal layer. These individual tetrahedral sites might be filled with one Li or one Ni ion if they share a face with a vacant octahedron in the transition metal layer. Although full occupancy of tetrahedral Li ions has been reported in

(38) Peres, J. P.; Weill, F.; Delmas, C. *Solid State Ionics* **1999**, *116*, 19.
(39) Arachi, Y.; Kobayashi, H.; Emura, S.; Nakata, Y.; Tanaka, M.; Asai, T. *Chem. Lett.* **2003**, *32*, 60.

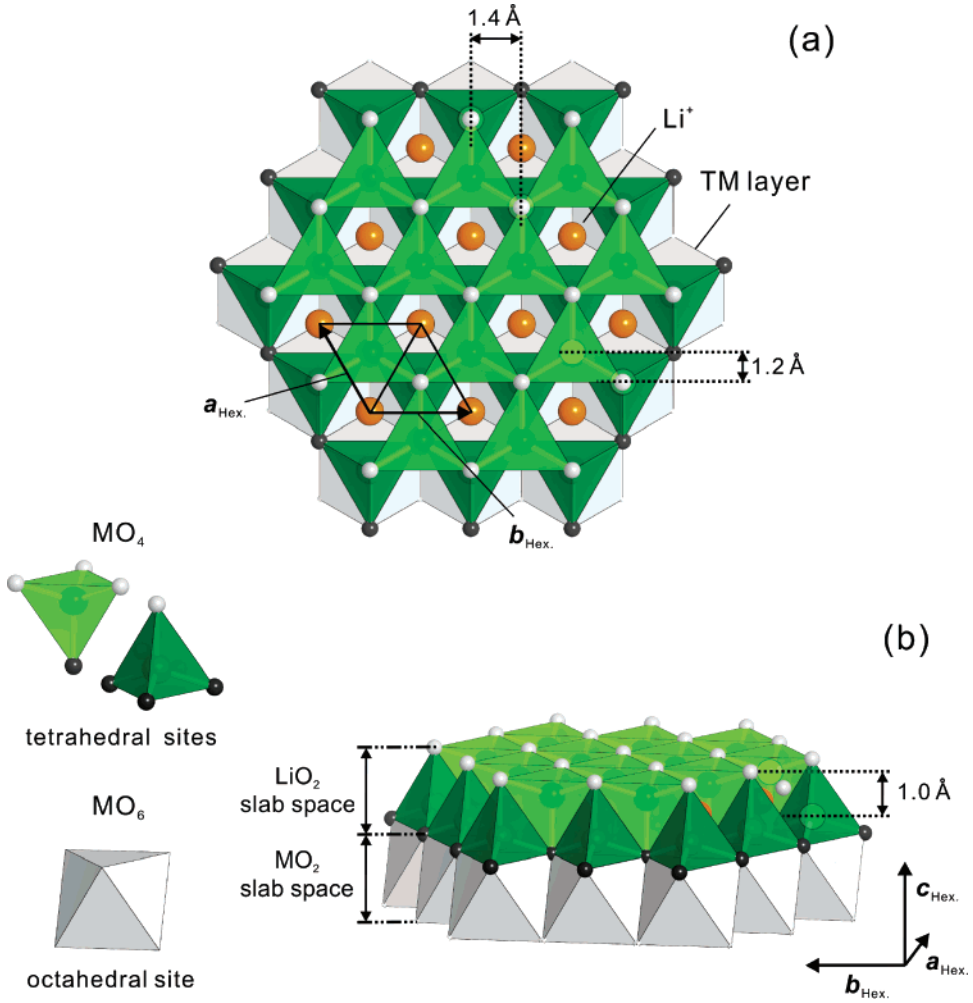

Figure 3. (a) Schematics of $Li_xNi_{0.5}Mn_{0.5}O_2$ structure viewed perpendicular to the transition metal slabs, where the parent hexagonal cell is outlined. Upper and lower tetrahedra in the Li layer, octahedral Li ions, and octahedra in the transition metal layer are shown; (b) schematics of $Li_xNi_{0.5}Mn_{0.5}O_2$ structure viewed along the $a_{Hex.}$ direction, where the upper and lower tetrahedral are revealed clearly.

Li_2NiO_2 with space group $P\bar{3}m1$,[40,41] the structure has a hexagonal closed-packed oxygen array (AB AB AB ...), where tetrahedral Li ions only share edges with the fully filled octahedral sites in the Ni layer. The distance between cations in the nearest upper and lower tetrahedral sites in $Li_xNi_{0.5}Mn_{0.5}O_2$ can be small, approximately 2.0−2.1 Å in the charged samples[12,29] if cations were placed close to the ideal position of the tetrahedral sites. Therefore, random occupancy of these tetrahedral sites and simultaneous occupancy of the nearest upper and lower tetrahedral sites should be unfavorable as a result of strong repulsive interactions between adjacent Ni and Li or Li and Li ions in the tetrahedral sites of the O3 structure (AB CA BC ...). A similar argument can be made about possible cation ordering on the octahedral sites in the discharged samples, which may result from electrostatic interactions between cations (Li and Ni) in the octahedral sites of the lithium layer. In this paper, we report electron diffraction data of $Li_xNi_{0.5}Mn_{0.5}O_2$ samples in the charged and discharge states, which were cycled to 4.5 V or 5.3 V. The changes in the $\sqrt{3}a_{Hex.} \times \sqrt{3}a_{Hex.} \times c_{Hex.}$ type long-range ordering in the transition metal layer are discussed with respect to reversible Ni movements between the Li layer and the transition metal layer upon charge and discharge. In addition, we show the formation of new long-range ordering in the charged and discharged samples, which are different from the $\sqrt{3}a_{Hex.} \times \sqrt{3}a_{Hex.} \times c_{Hex.}$ type, and discuss possible ordered cation arrangements in the layered $Li_xNi_{0.5}Mn_{0.5}O_2$ structure.

Experimental Section

The pristine $LiNi_{0.5}Mn_{0.5}O_2$ sample was synthesized from the following steps: (1) nickel and manganese hydroxides were obtained from $Ni(NO_3)_2$ and $Mn(NO_3)_2$ with LiOH solution; (2) a stoichiometric amount of $LiOH{\cdot}H_2O$ was added to Ni and Mn hydroxides, and the mixture was heated at 480 °C for 12 h in air; (3) a pellet was then made from the product; and (4) the pellet was heated at 1000 °C for 12 h in air and was quenched to room temperature between two thick copper plates.

The reversible capacities and electrochemical activity of $LiNi_{0.5}Mn_{0.5}O_2$ composite electrodes were measured in 2016 coin cells that have lithium foil as the negative electrode. Detailed electrode preparation and the 2016 coin cell assembly procedure can be found from a relevant study.[42] $Li_xNi_{0.5}Mn_{0.5}O_2$ exhibits 180−185 (mA h)/g of initial rechargeable capacity at C/50 in the voltage range of

(40) Dahn, J. R.; Vonsacken, U.; Michal, C. A. *Solid State Ionics* **1990**, *44*, 87.
(41) Davidson, I.; Greedan, J. E.; Vonsacken, U.; Michal, C. A.; Dahn, J. R. *Solid State Ionics* **1991**, *46*, 243.
(42) Yabuuchi, N; Sundeep, K.; Li, H. H.; Kim, Y.-T.; Shao-Horn, Y. *J. Electrochem. Soc.* **2006**, in press.

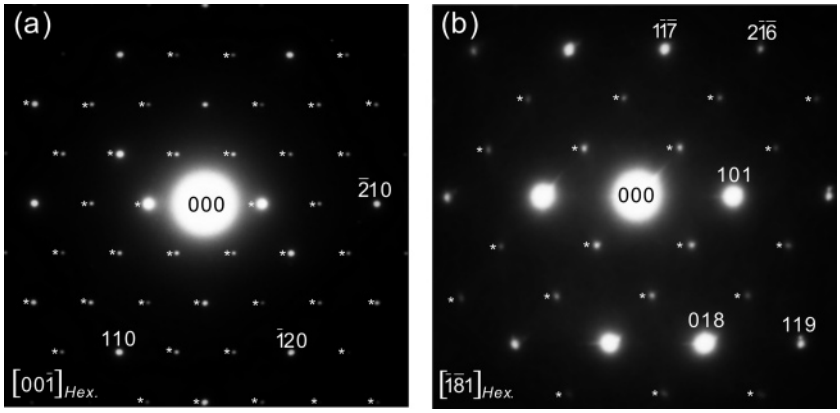

Figure 4. Experimental electron diffraction patterns collected from the pristine $LiNi_{0.5}Mn_{0.5}O_2$ sample, which are indexed along the (a) $[00\bar{1}]_{Hex.}$ zone axis and (b) $[\bar{1}\bar{1}81]_{Hex.}$ zone axis. Superlattice reflections consistent with the $\sqrt{3}a_{Hex.} \times \sqrt{3}a_{Hex.} \times c_{Hex.}$ supercell are marked by white stars.

2.0 to 4.5 V at room temperature (typically 20 − 25 °C), as shown in Figure 2. In addition, discharge capacities for the first 25 cycles collected at various current densities in the same voltage range are shown as an inset in Figure 2, where no significant loss in the capacity is noted upon cycling. Electrodes made from the pristine sample have reproducible electrochemical behavior as shown from the results of four duplicate cells. This rechargeable capacity is slightly smaller than that reported by Makimura and Ohzuku[5] (approximately 200 (mA h)/g in the voltage range of 2.5 to 4.55 V at 30 °C). It should be noted that electrochemical cycling conditions such as cycling voltage limit and temperature in this study are not identical to those used in previous studies[5] including the voltage range. As charging up to higher voltage can lead to larger reversible capacities at the same current density and then higher temperature also increases reversible capacities,[2] it is believed that the pristine $LiNi_{0.5}Mn_{0.5}O_2$ sample used in this study can have electrochemically activity comparable to the samples reported previously.[5]

Two samples charged to 4.5 and 5.3 V after two complete cycles and two discharged samples that that were cycled to 4.5 and 5.3 V for five complete cycles were selected for electron and synchrotron X-ray powder diffraction experiments. To ensure sample homogeneity, electrochemical cycling was conducted at a *C*/50 rate (0.027 mA/cm^2). The compositions of the 4.5 V charged and discharged samples were estimated to be $Li_{0.2}Ni_{0.5}Mn_{0.5}O_2$ and $Li_{0.9}Ni_{0.5}Mn_{0.5}O_2$ by assuming 100% Columbic efficiency upon charge and discharge, respectively. However, the Li compositions in the 5.3 V charged and discharged sample cannot be estimated accurately as a result of electrolyte decomposition at voltages greater than ∼4.6 V (Figure 2). It is believed that the 5.3 V charged sample had a composition of $Li_xNi_{0.5}Mn_{0.5}O_2$ ($x = \sim 0$) and the 5.3 V discharged sample had a Li content, *x*, equal to or greater than ∼0.8 by assuming 100% Columbic efficiency upon the last discharge.

Cycled $Li_xNi_{0.5}Mn_{0.5}O_2$ electrodes were recovered from the coin cells inside the glovebox, which were then rinsed thoroughly with diethyl carbonate to remove the electrolyte salt. Transmission electron microscopy (TEM) samples were prepared by suspending the powder from the positive electrodes onto a copper grid with lacy carbon. Single crystal selected area electron diffraction patterns were collected from the samples under an accelerating voltage of 200 keV on a JEOL 200CX or JEOL 2010 microscope. Selected area electron diffraction patterns were collected from 20 to 30 randomly selected single crystals within each sample, which were obtained from multiple electron diffraction experiments. Simulation of single-crystal electron diffraction and X-ray powder diffraction patterns was performed using CaRIne Crystallography software. Electron diffraction data were compared with the Rietveld refinement results from synchrotron X-ray diffraction data detailed in a earlier study,[42] which were collected on samples identical to those used in the electron diffraction experiments or samples extracted from duplicate cells.

Results

Pristine $LiNi_{0.5}Mn_{0.5}O_2$. Single crystal selected area electron diffraction patterns were collected from 20 randomly selected crystals of the pristine $LiNi_{0.5}Mn_{0.5}O_2$ sample, of which 95% show superlattice reflections that evidence long-range ordering in the transition metal layer, consistent with previous studies.[18,19,42] Two representative patterns collected along the $[00\bar{1}]_{Hex.}$ and $[\bar{1}\bar{1}81]_{Hex.}$ zone axes are shown in Figure 4a,b, respectively. In addition to fundamental reflections of the parent hexagonal cell with space group $R\bar{3}m$, superlattice reflections (marked by stars in Figure 4a,b) were observed. These superlattice reflections could be indexed consistently to the $\sqrt{3}a_{Hex.} \times \sqrt{3}a_{Hex.} \times c_{Hex.}$ superstructure with space group $P3_112$,[18,19] where the crystallographic relationship between the parent and the superstructure has been described in detail previously.[19] The $(11l)_{Hex.}$ planar spacings ($l = 3n$, $n = 0, \pm1, \pm2, ...$) in the parent hexagonal structure are tripled by the presence of superlattice reflections, which is in good agreement with the simulated patterns (See Supporting Information Figures S1a,b for simulated electron diffraction patterns). The appearance of these superlattice reflections is indicative of ordering of the cations in the transition metal layer into the Li-rich and Li-deficient sites in the trigonal lattice.[18,19]

Electrochemically Charged $Li_xNi_{0.5}Mn_{0.5}O_2$ Samples. Electron diffraction patterns were collected from 26 randomly selected crystals in each of the charged samples to 4.5 V ($Li_{0.2}Ni_{0.5}Mn_{0.5}O_2$) and to 5.3 V ($Li_xNi_{0.5}Mn_{0.5}O_2$ and $x = \sim 0$). Electron diffraction patterns of these charged samples were examined, and the observed superlattice reflections differed from the pristine sample in the following three ways. First, a significant percentage of the crystals in these charged samples no longer exhibited superlattice reflections of the $\sqrt{3}a_{Hex.} \times \sqrt{3}a_{Hex.} \times c_{Hex.}$ type. Second, a fraction of the crystals showed the appearance of superlattice reflections that leads to doubling of some interplanar spacings in the parent structure, which cannot be indexed to the $\sqrt{3}a_{Hex.} \times \sqrt{3}a_{Hex.} \times c_{Hex.}$ supercell. The appearance of these superlattice

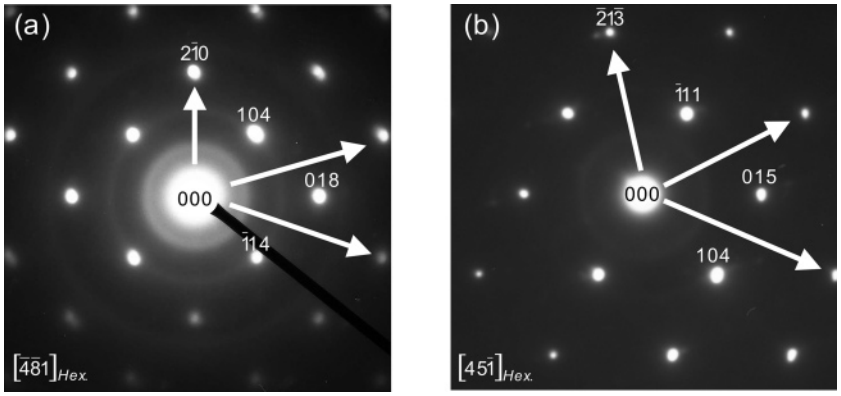

Figure 5. Experimental electron diffraction patterns exhibiting only fundamental reflections collected (a) from the 4.5 V charged sample ($Li_{0.2}Ni_{0.5}Mn_{0.5}O_2$), which is indexed to the $[\bar{4}\bar{8}1]_{Hex.}$ zone axis, and (b) from the 5.3 V charged sample ($Li_xNi_{0.5}Mn_{0.5}O_2$, $x = \sim 0$) sample, which is indexed to the $[45\bar{1}]_{Hex.}$ zone axis. Superlattice reflections expected for the $\sqrt{3}a_{Hex.} \times \sqrt{3}a_{Hex.} \times c_{Hex.}$ supercell in the marked reciprocal directions have disappeared.

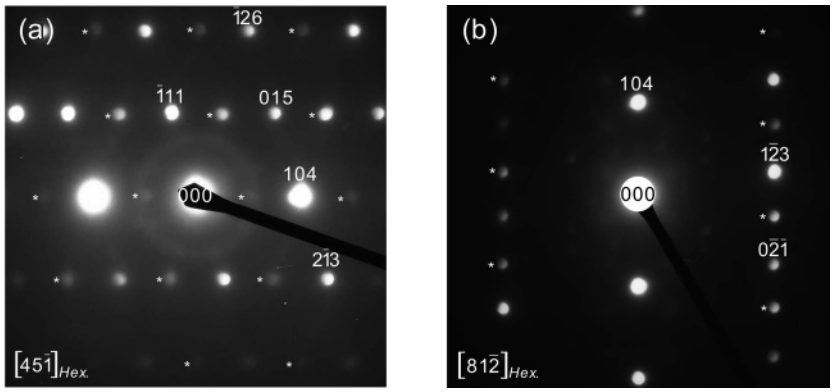

Figure 6. Experimental electron diffraction patterns exhibiting doubling superlattice reflections collected from the charged $Li_{0.2}Ni_{0.5}Mn_{0.5}O_2$ sample to 4.5 V along the (a) $[45\bar{1}]_{Hex.}$ zone axis and the (b) $[81\bar{2}]_{Hex.}$ zone axis.

reflections is more predominant in the 4.5 V charged sample than in the 5.3 V charged sample. Finally, superlattice reflections unique to the O1 phase, which were reported previously for highly de-intercalated Li_xCoO_2[32] and Li_xNiO_2[37,43] ($x = \sim 0$) samples, were found in some patterns collected from the 5.3 V charged sample but not in the 4.5 V charged sample.

Disappearance of the $\sqrt{3}a_{Hex.} \times \sqrt{3}a_{Hex.} \times c_{Hex.}$ Superlattice Reflections. Not only were the intensities of the $\sqrt{3}a_{Hex.} \times \sqrt{3}a_{Hex.} \times c_{Hex.}$ superlattice reflections in the 4.5 and 5.3 V charged samples weakened considerably in comparison to those observed for the pristine sample, and a significant fraction of crystals exhibited only fundamental reflections of the parent structure. Representative electron diffraction patterns from the 4.5 and 5.3 V charged samples along the $[\bar{4}\bar{8}1]_{Hex.}$ and $[45\bar{1}]_{Hex.}$ zone axes are shown in Figure 5a,b, respectively. Superlattice reflections that are expected for the $\sqrt{3}a_{Hex.} \times \sqrt{3}a_{Hex.} \times c_{Hex.}$ supercell in the marked reciprocal directions were not observed. In addition, the 5.3 V charged sample having many fewer crystals (~19%) showed the $\sqrt{3}a_{Hex.} \times \sqrt{3}a_{Hex.} \times c_{Hex.}$ superlattice reflections than the 4.5 V charged sample (~58%). The weakening and disappearance of these superlattice reflections in the charged samples reflect decreased contrast in the averaged electron scattering factor between the Li-rich and Li-deficient sublattices of the $\sqrt{3}a_{Hex.} \times \sqrt{3}a_{Hex.} \times c_{Hex.}$ superstructure.[18] This observation is indicative of changes in the long-range ordering in the transition metal layer of $Li_xNi_{0.5}Mn_{0.5}O_2$ during Li de-intercalation (upon charging), which will be discussed in detail in later sections.

Appearance of Doubling Superlattice Reflections. In addition to the disappearance of the $\sqrt{3}a_{Hex.} \times \sqrt{3}a_{Hex.} \times c_{Hex.}$ superlattice reflections, extra reflections that were indicative of doubling of some interplanar spacings of the parent structure, such as the $(10l)_{Hex.}$ and $(11l)_{Hex.}$ planar spacings ($l = 2n$, $n = 0, \pm 1, \pm 2, ...$), were noted in the charged samples. The presence of these superlattice reflections is indicative of long-range ordering of cations in a hexagonal $2a_{Hex.} \times 2a_{Hex.} \times c_{Hex.}$ supercell or a monoclinic $a_{Mon.} \times a_{Mon.} \times c_{Mon.}$ primitive cell analogous to that reported previously for $Li_{0.5}CoO_2$.[22] Two representative electron diffraction patterns from the 4.5 V charged sample collected along the $[45\bar{1}]_{Hex.}$ and $[81\bar{2}]_{Hex.}$ zone axes are shown in Figure 6a,b, respectively. Fundamental reflections of the parent structure are indexed while superlattice reflections (marked by stars) cannot be indexed consistently to the $\sqrt{3}a_{Hex.} \times \sqrt{3}a_{Hex.} \times c_{Hex.}$ supercell (see simulated electron diffraction patterns in Supporting Information Figure S2a,b). It should be mentioned that these types of superlattice reflections were found to coexist with those of the $\sqrt{3}a_{Hex.} \times \sqrt{3}a_{Hex.} \times c_{Hex.}$ supercell in some crystals of the 4.5 V charged sample. Similar superlattice reflections were found in much fewer crystals of the 5.3 V charged sample. Two representative patterns are shown in Figure 7a,b, which are

(43) Croguennec, L.; Pouillerie, C.; Delmas, C. *Solid State Ionics* **2000**, *135*, 259.

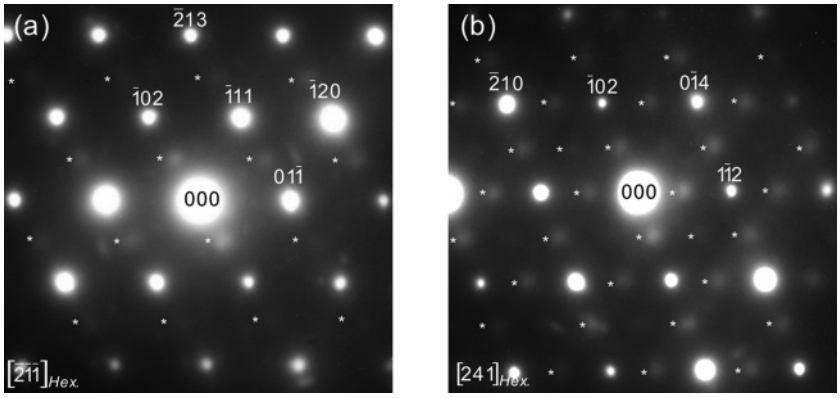

Figure 7. Experimental electron diffraction patterns exhibiting doubling superlattice reflections collected from the charged $Li_xNi_{0.5}Mn_{0.5}O_2$ ($x = \sim 0$) sample to 5.3 V along the (a) $[\bar{2}\bar{1}\bar{1}]_{Hex.}$ zone axis and the (b) $[241]_{Hex.}$ zone axis.

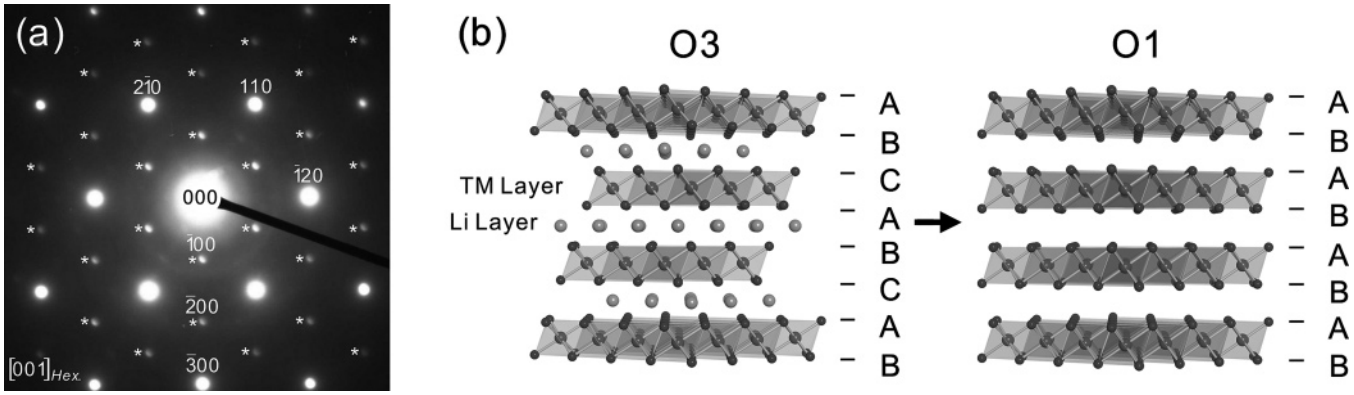

Figure 8. (a) Experimental electron diffraction patterns of the O1 phase collected from charged $Li_xNi_{0.5}Mn_{0.5}O_2$ ($x = \sim 0$) sample to 5.3 V along the $[001]_{Hex.}$ zone axis. (b) Schematics of the O3 with cubic-close-packed oxygen arrays and the O1 structure with hexagonal-close-packed oxygen arrays.

indexed to the $[\bar{2}\bar{1}\bar{1}]_{Hex.}$ and $[241]_{Hex.}$ zone axes, respectively. They cannot be explained consistently by the $\sqrt{3}a_{Hex.} \times \sqrt{3}a_{Hex.} \times c_{Hex.}$ supercell (see simulated patterns in Supporting Information Figure S3a,b). It should be noted that doubling superlattice reflections of $(104)_{Hex.}$ are either extremely weak relative to other superlattice reflections (Figure 6a) or not visible (Figure 6b) in the charged samples. For example, the $[241]_{Hex.}$ zone axis pattern in Figure 7b clearly shows doubling superlattice reflections (marked by white stars) of the $(10\bar{2})_{Hex.}$ and $(110)_{Hex.}$ planes, while those of $(104)_{Hex.}$ are not observable. Possible long-range cation ordering, which is responsible for the appearance of these superlattice reflections in the charged samples, will be discussed in detail in later sections.

Appearance of Extra Reflections for the O1 $a_{Hex.} \times a_{Hex.} \times c_{Hex.}$ Cell. Additional reflections (marked by white stars), indicative of a primitive $a_{Hex.} \times a_{Hex.} \times c_{Hex.}$ cell, were found in the $[001]_{Hex.}$ pattern collected from the 5.3 V charged sample, as shown in Figure 8a. The pattern cannot be indexed to the $\sqrt{3}a_{Hex.} \times \sqrt{3}a_{Hex.} \times c_{Hex.}$ supercell. These extra reflections were found one-third of the way between the diffraction center and the $(300)_{Hex.}$ fundamental reflections. They can be indexed consistently to the O1 structure with AB AB AB ... oxygen packing having the space group $P\bar{3}m1$ (see Supporting Information Figure S4). Electron diffraction evidence of the O1 formation in the 5.3 V charged $Li_xNi_{0.5}Mn_{0.5}O_2$ sample ($x = \sim 0$) is further supported by recent synchrotron X-ray diffraction data, which reveal three small diffraction peaks unique to the O1 phase and the coexistence of primary O3 and minor O1 (~10% by volume) phases in the 5.3 V charged sample in the synchrotron X-ray data.[42] It should be noted that both the electron diffraction and synchrotron X-ray diffraction data are not consistent with the H1-3 structure. The O1 phase was not so clearly observed in the neutron diffraction study of the 5.3 V charged sample, because most of the reflections unique to O1, were hidden under the reflections due to graphite (which was added to cathode material in this study).[27] Careful inspection of the neutron diffraction pattern of the 5.2 V charged sample after the work was reported[27] did, however, reveal the presence of a small concentration of the O1 phase. Removal of all Li and Ni ions in the Li layer leads to the sliding of transition metal slabs that forms the O1 structure with hexagonal-close-packed oxygen arrays, which is shown in Figure 8b. As expected, the O1 phase was not found in the 4.5 V charged sample ($Li_{0.2}Ni_{0.5}Mn_{0.5}O_2$) as a considerable amount of lithium remains in the layered structure. Electron diffraction simulation analyses show that the parent O3 structure with space group $R\bar{3}m$ and the O1 phase with space group $P\bar{3}m1$ have similar patterns along many zone axes, which cannot be distinguished by electron diffraction data of this study. Therefore, patterns that have zone axes other than $(001)_{Hex.}$, which do not exhibit any superlattice reflections, can be indexed to either the O3 or the O1 structure. The observation of the O1 phase is consistent with the notion of Ni migration from the Li layers, as any residual Ni would be expected to pin the transition metal slabs, preventing O1 formation.

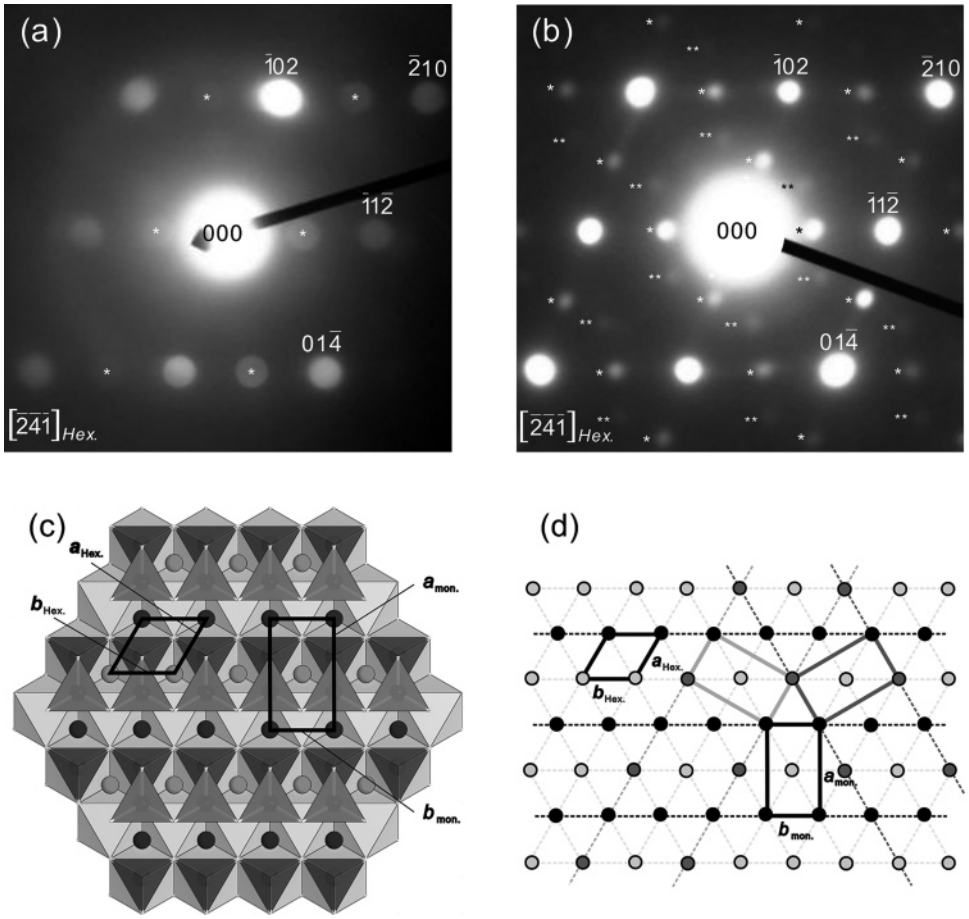

Figure 9. (a, b) Two different experimental electron diffraction patterns collected from the 4.5 V discharged sample, which are indexed along the $[\bar{2}4\bar{1}]_{Hex.}$ zone axis. Doubling and tripling superlattice reflections are marked by one and two stars, respectively. (c) Proposed cation ordering in the $a_{Mon.} \times a_{Mon.} \times c_{Mon.}$ supercell with space group $P2/m$ and (d) three variants of the proposed ordering.

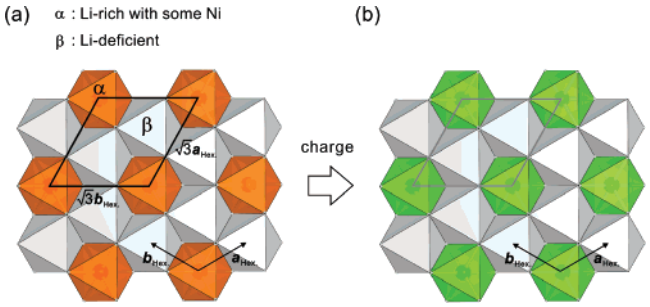

Figure 10. Schematics of (a) $\sqrt{3}a_{Hex.} \times \sqrt{3}a_{Hex.} \times c_{Hex.}$ ordering of Li-rich and Li-deficient sites in the transition metal layer in the pristine sample and (b) such ordering in the charged samples after Ni ions migrate into previously Li-rich sites in the transition metal layer upon charging. The intensity reduction of the superlattice reflections is a result of the decreasing contrast between the α and β sites.

Electrochemically Discharged $Li_xNi_{0.5}Mn_{0.5}O_2$. Electron diffraction patterns were collected from 25 randomly selected crystals of the $Li_{0.9}Ni_{0.5}Mn_{0.5}O_2$ sample that was discharged to 2.0 V from 4.5 V and from 20 crystals from the discharged $Li_xNi_{0.5}Mn_{0.5}O_2$ sample (after cycling to 5.3 V; $x > 0.76$). Similar types of superlattice reflections were observed in the discharged samples as compared to the charged samples. It was found that ~80% and ~55% of the crystals exhibited the $\sqrt{3}a_{Hex.} \times \sqrt{3}a_{Hex.} \times c_{Hex.}$ superlattice reflections in the 4.5 and 5.3 V discharged samples, respectively. In addition, ~28% of the crystals from the 4.5 V discharged sample and ~35% of the crystals from the 5.3 V discharged sample showed the doubling superlattice reflections. Moreover, none of the patterns collected from the discharged samples exhibited the additional reflections that are consistent with the O1 structure.

A number of electron diffraction patterns in the discharged samples can be indexed to either a hexagonal $2a_{Hex.} \times 2a_{Hex.} \times c_{Hex.}$ supercell or a monoclinic $a_{Mon.} \times a_{Mon.} \times c_{Mon.}$ primitive cell. Quite a few electron diffraction patterns with doubling superlattice reflections show unique evidence for cation ordering in the $a_{Mon.} \times a_{Mon.} \times c_{Mon.}$ cell. For example, one of the $[\bar{2}4\bar{1}]_{Hex.}$ zone axis patterns collected from the 4.5 V discharged sample is shown in Figure 9a, where doubling superlattice reflections of the $(10\bar{2})_{Hex.}$ planes are present and those of $(110)_{Hex.}$ and $(104)_{Hex.}$ are clearly absent. The absence of doubling superlattice reflections of the $(110)_{Hex.}$ planes in this zone axis excludes the $2a_{Hex.} \times 2a_{Hex.} \times c_{Hex.}$ supercell. It is also interesting to note that doubling superlattice reflections of $(104)_{Hex.}$ are either weak or absent in the discharged samples. Discussion of possible cation distributions and long-range ordering will be presented in detail in the next section.

Discussion

Evidence for Nickel Migration upon Cycling. *Nickel Migration from the Li to the Transition Metal Layer upon Charging.* In the pristine $LiNi_{0.5}Mn_{0.5}O_2$ sample, Li, Mn, and Ni ions in the transition metal layer are ordered into Li-rich

and Li-deficient sites in the trigonal lattice, as shown in Figure 10a. The contrast in the average scattering intensities of these two sites gives rise to the $\sqrt{3}a_{Hex.} \times \sqrt{3}a_{Hex.} \times c_{Hex.}$ superlattice reflections as shown in Figure 4a,b and by previous studies.[18,19] Li MAS NMR studies[10] have revealed that Li ions can be removed from both Li and transition metal layers and that all of the Li in the transition metal layer can be removed upon charging to $Li_{0.40}Ni_{0.5}Mn_{0.5}O_2$. De-intercalated Li ions create vacant sites in the transition metal layers, which would slightly increase the contrast in the average scattering factor between these two sites as compared to that in the pristine sample and would not lead to reduced intensities of the $\sqrt{3}a_{Hex.} \times \sqrt{3}a_{Hex.} \times c_{Hex.}$ superlattice reflections. Experimentally observed weakening or disappearance of these superlattice reflections in the charged samples is indicative of decreasing long-range ordering in the transition metal layer. Reduced ordering in the $\sqrt{3}a_{Hex.} \times \sqrt{3}a_{Hex.} \times c_{Hex.}$ supercell might be attributed to the following two scenarios upon charging: (1) in-plane movements of Ni and Mn ions in the transition metal layer, which result in a random distribution of Ni, Mn, and vacancies, and (2) Ni migration from the Li layer to fill the vacant sites left behind by de-intercalated Li ions in the transition metal layer. Both cases can decrease the contrast in the average scattering intensity between these two sites in comparison to that of the pristine sample, as shown in Figure 10b. Synchrotron X-ray powder diffraction analyses[42] of these charged samples reveal a significant increase in the Ni occupancy (octahedral 3a sites) of the transition metal layer. Cation occupancies in the octahedral and tetrahedral sites found in the pristine and 4.5 V charged ($Li_{0.2}Ni_{0.5}Mn_{0.5}O_2$) samples are shown in Figure 11a. Therefore, both synchrotron X-ray powder diffraction and electron diffraction results support the concept of the onset of Ni migration from the Li layer into vacant sites in the transition metal layer even upon charging to voltages equal to or lower than 4.5 V.

Oxidation of Ni^{2+} ions in the Li layer, having similar ionic radii to Li^+ ions, to smaller Ni^{3+} (0.56 Å) or Ni^{4+} (0.48 Å) ions is not favored relative to those in the transition metal layer. In particular, the Li (LiO_2) slab space is increased considerably upon charging (~6% to 4.5 V), while the transition metal slab space is reduced (~6% to 4.5 V), as shown in Figure 11b. Ni^{3+} and Ni^{4+} ions are likely to be more stable in the transition metal layer than in the Li layer in the samples charged to these high voltages. Therefore, similar to previous studies in lithium nickel oxides,[26] it is hypothesized that Ni^{2+} ions in the transition metal layer are preferentially oxidized relative to those in the Li layer upon charging. Ni^{2+} in the Li layer could move into the tetrahedral sites that face share with a vacant octahedral site in the transition metal layer, migrate, and fill the octahedral vacancy upon further oxidation to Ni^{3+} or Ni^{4+} as suggested previously.[27,42]

The fraction of crystals exhibiting the $\sqrt{3}a_{Hex.} \times \sqrt{3}a_{Hex.} \times c_{Hex.}$ superlattice reflections can be indicative of the amount of Ni ions that have migrated into the transition metal layer upon cycling. The fraction of crystals showing the $\sqrt{3}a_{Hex.} \times \sqrt{3}a_{Hex.} \times c_{Hex.}$ superlattice reflections is significantly reduced upon charging to 4.5 V in Figure 12, which is consistent with the increased Ni occupancy in the transition metal layer from Rietveld refinement in Figure 11a. It should

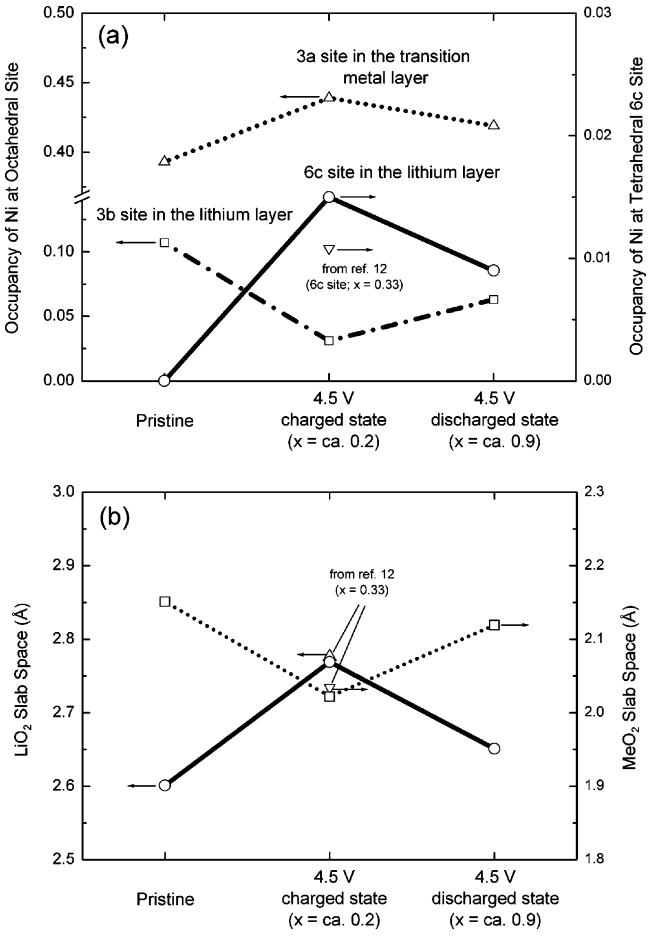

Figure 11. (a) Ni occupancy in the octahedral and tetrahedral sites and (b) the change in LiO_2 and MeO_2 slab space obtained from Rietveld analysis of synchrotron X-ray diffraction patterns of the pristine, charged 4.5 V, and discharged 4.5 V samples (details can be found in an earlier study[42]). The samples used for synchrotron X-ray powder diffraction experiments were either identical to those used for electron diffraction or obtained from duplicate cells. A $Li_{0.33}Ni_{0.5}Mn_{0.5}O_2$ sample obtained from charging to 4.3 V reported previously[12] is also shown for comparison.

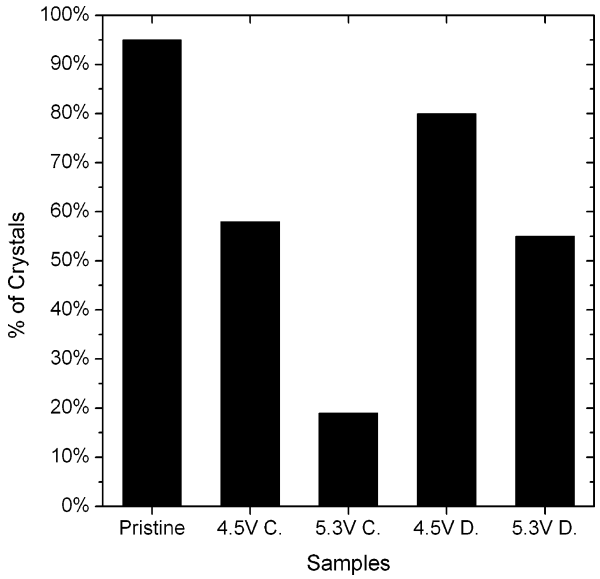

Figure 12. Comparison of the percentage of crystals exhibiting the $\sqrt{3}a_{Hex.} \times \sqrt{3}a_{Hex.} \times c_{Hex.}$ type superlattice reflections in the pristine, 4.5 V charged, 5.3 V charged, 4.5 V discharged, and 5.3 V discharged samples.

be mentioned, however, that the recent neutron diffraction analyses showed no evidence for significant Ni migration to the transition metal layer in an electrode sample charged to 4.6 V. As the extent of Ni migration is strongly correlated to Li content and valence state of Ni in $Li_xNi_{0.5}Mn_{0.5}O_2$, this discrepancy can be attributed to the fact that the charged sample used for neutron diffraction had a considerably higher Li amount ($Li_{0.33}Ni_{0.5}Mn_{0.5}O_2$) than the electrode ($Li_{0.2}Ni_{0.5}Mn_{0.5}O_2$) charged to 4.5 V in this study. Upon charging from 4.5 to 5.3 V, the fraction of crystals exhibiting the $\sqrt{3}a_{Hex.} \times \sqrt{3}a_{Hex.} \times c_{Hex.}$ superlattice reflections is reduced further, as shown in Figure 12. This observation suggests that charging to voltages higher than 4.5 V induces additional Ni ions to migrate into the transition metal layer. This is in good agreement with the decrease in Ni occupancy in the Li layers from ~0.10 to 0.024 per formula unit seen by neutron diffraction upon charging to 5.2 V with a final composition of $Li_{0.06}Ni_{0.5}Mn_{0.5}O_2$.[27] In some crystals of the 5.3 V charged sample, all of the Ni ions in the Li layer may be removed and displaced into vacant octahedral sites in the transition metal layer as evidenced by the appearance of the O1 phase in some crystals of the 5.3 V charged sample (Figure 8), where nearly all of the Li ions are removed and nearly all of Ni ions are oxidized to Ni^{4+} and located in the transition metal layer.

The process of Ni migration can occur over a wide range of voltages upon charging. The onset of Ni migration occurs at voltages equal to or lower than 4.5 V, and some Ni ions remain in the Li layer even upon charging to 5.3 V, as evidenced by electron diffraction (Figure 12) and synchrotron X-ray powder diffraction data.[42] The magnitude of the voltage that can induce Ni migration from the Li layer to the transition metal layer via the tetrahedral sites may depend on local cation arrangements of Ni in the Li layer. If a Ni^{2+} ion were located in an octahedral site in the Li layer, sharing an edge with a vacant octahedral site in the transition metal layer (Figure 2), it could hop into the adjacent tetrahedral site of the Li layer that is face sharing with the vacant octahedral site.[28] Ni^{2+} ions in these tetrahedral sites have been shown to move into the vacant octahedral site in the transition metal layer upon oxidation without any energy barrier.[27] They may move into the transition metal layer at voltages equal to or lower than 4.5 V. However, if an octahedral Ni ion in the Li layer did not edge share with octahedral vacancy in the transition metal layer (for example, only shared corners with octahedral vacancies in the transition metal layer), migration of such Ni ions would be kinetically difficult as they need to go through adjacent tetrahedral sites in the Li layer, which face share with adjacent, filled octahedral sites in the transition metal layer. First-principles studies have shown the activation barrier for Ni hopping through such tetrahedral sites can be as high as 1 eV.[27] These Ni ions in the Li layer that are positioned more distant from octahedral vacancies in the transition metal layer may migrate upon charging to voltages considerably higher than 4.5 V. Local environments of octahedral Ni in the Li layer with and without an edge-shared octahedral vacancy in the transition metal layer will vary from region to region within one crystal and from crystal to crystal in the $Li_xNi_{0.5}Mn_{0.5}O_2$ samples. This argument is in agreement with our observations that the intensities of the $\sqrt{3}a_{Hex.} \times \sqrt{3}a_{Hex.} \times c_{Hex.}$ superlattice reflections vary among different crystals in the charged samples, and only a fraction of the $Li_xNi_{0.5}Mn_{0.5}O_2$ crystals has transformed to the O1 phase (indicating significant migration of the Ni ions from the Li layer to the transition metal layer in these crystals) upon charging to 5.3 V.

Ni Migration from the Transition Metal to Li Layer upon Discharge. Ni migration appears to be in part reversible upon discharge. The fractions of crystals with the $\sqrt{3}a_{Hex.} \times \sqrt{3}a_{Hex.} \times c_{Hex.}$ superlattice reflections in the discharged samples are considerably higher than those of charged samples, as shown in Figure 12. This observation suggests that a fraction of Ni ions that migrate into the transition metal layer upon charging moves back to the Li layer upon discharge. Although some Ni ions move back to the Li layer upon discharge, the discharged samples[42] have reduced interlayer mixing and increased Ni occupancy in the transition metal layer in comparison to the pristine sample, as shown in Figure 11a. This result is consistent with recent X-ray and neutron diffraction analyses of discharged electrodes cycled to 5.2 V,[27] where the fraction of Ni ions in the Li layer is reduced by ~4% per formula unit relative to the pristine sample. Recent first-principles and NMR results have suggested that the stability of Ni ions in the transition metal layer may be dependent on its nearest cation neighbors and may decrease with increasing Mn^{4+} neighbors.[27] It has been proposed that Ni^{4+} surrounded by six Mn^{4+} are the most likely to migrate back to the Li layer upon discharge.[27]

After cycling to 5.3 V, fewer crystals in the discharged electrode exhibit the $\sqrt{3}a_{Hex.} \times \sqrt{3}a_{Hex.} \times c_{Hex.}$ superlattice reflections in comparison to the 4.5 V discharged electrode (Figure 12). This observation may suggest that more Ni ions are permanently displaced into the transition metal layer in the 5.3 V discharged sample in comparison to electrodes cycled to 4.5 V. Our electron diffraction observations are in agreement with electrochemical cycling results, which show that electrodes first exposed to 5.3 V have improved reversible capacities and rate capability during subsequent cycling to 4.5 V.[42] Increasing layered character (reducing cation disorder or interlayer mixing) can enhance the rate capability of similar layered compounds as shown recently by studies of ion-exchanged $LiNi_{0.5}Mn_{0.5}O_2$[15] and $LiNi_{0.56}Mn_{0.44}O_2$ samples,[44] which have small amounts of cation disorder (~0.04−0.06 per formula unit).

The physical origin of the ifference in the Ni stability between the 4.5 and the 5.3 V charged samples is not fully understood. We postulate that structural differences between these two samples may influence Ni stability in the adjacent, face-shared tetrahedral sites in the Li layer upon discharge, which may play a key role in the Ni stability in the transition metal layer. The occupancy of Li (as revealed by recent neutron diffraction data)[27] and Ni (Figure 11a) ions in the tetrahedral sites of the Li layer in the 4.5 V charged sample is accompanied by a relatively large Li slab space, as shown

(44) Schougaard, S. B.; Breger, J.; Jiang, M.; Grey, C. P.; Goodenough, J. B. *Adv. Mater.* **2006**, *18*, 905.

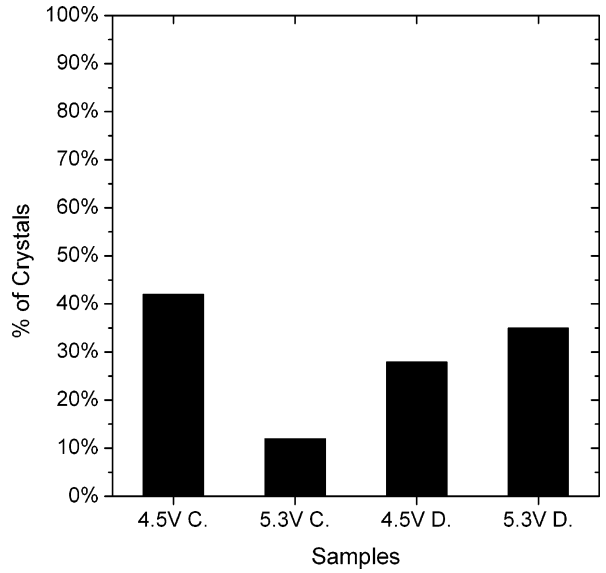

Figure 13. Comparison of the percentage of crystals that exhibit doubling superlattice reflections in the pristine, 4.5 V charged, 5.3 V charged, 4.5 V discharged, and 5.3 V discharged samples.

in Figure 11b. Such a large Li slab space may allow Ni ions to move out of octahedral sites in the transition metal layer and occupy adjacent, face-shared tetrahedral sites in the Li layer upon reduction to Ni^{2+} during the initial discharge and migrate into the Li layer upon further lithium intercalation. Although the Li slab space of the O1 $Ni_{0.5}Mn_{0.5}O_2$ phase could not be obtained from refinement of synchrotron X-ray powder diffraction data,[42] the O1 structure has a much smaller distance between adjacent transition metal layers (4.68 Å) than that (4.72 Å) in the O3 structure of the 5.3 V charged sample. This observation is in good agreement with previous studies in that O1 CoO_2[32] and O1 NiO_2[37,43] structures exhibit a markedly reduced lattice parameter $c_{Hex.}$ than observed in the slightly intercalated phases. Assuming that the thickness of the transition metal slabs is primarily determined by the valence of Ni and Mn, one may argue that the large change in the lattice parameter $c_{Hex.}$ or the distance between adjacent transition metal layers results from considerable reduction in the Li slab space. In addition, the Li slab space (4.79 Å) in the O3 structure of the 4.5 V charged sample is much larger than those of the O3 and O1 phases in the 5.3 V charged sample. Therefore, it is hypothesized that small Li slab space may lead to undesirable Ni−O bond length in the tetrahedral sites and make reverse Ni migration from octahedral sites in the transition metal layer to adjacent, face-sharing tetrahedral sites unfavorable upon reduction to Ni^{2+} during the initial discharge. This may stabilize more Ni ions in the transition metal layer in the 5.3 V discharged sample relative to that cycled to 4.5 V.

Evidence of New Long-Range Ordering of Cations in Cycled $Li_xNi_{0.5}Mn_{0.5}O_2$. The fractions of crystals in the charged samples, which exhibit doubling superlattice reflections of the hexagonal $2a_{Hex.} \times 2a_{Hex.} \times c_{Hex.}$ or the monoclinic $a_{Mon.} \times a_{Mon.} \times c_{Mon.}$ type, are summarized in Figure 13. These superlattice reflections were found much more prevalent in the 4.5 V charged sample (~42%) in comparison to the 5.3 V charged sample (~12%). The 4.5 and 5.3 V discharged samples had similar fractions of crystals that showed superlattice reflections of the monoclinic $a_{Mon.} \times a_{Mon.} \times c_{Mon.}$ type. Long-range ordering of Li, Ni, and vacancy in the tetrahedral and octahedral sites of the Li layer can give rise to the appearance of similar superstructures.

Proposed Models of Tetrahedral and Octahedral Ordering. Long-range ordering of one cation-rich and one cation-deficient site in the tetrahedral and octahedral sites of the Li layer can give rise to doubling superlattice reflections of the $2a_{Hex.} \times 2a_{Hex.} \times c_{Hex.}$ and $a_{Mon.} \times a_{Mon.} \times c_{Mon.}$ types. Here we introduce and discuss four different structural models, as shown in Figure 14a−d. Upper (pointing down) and lower (pointing up) tetrahedral sites may be occupied partially by Li or Ni every other row in Figure 14a. In this first model, octahedral cations and vacancies can be randomly distributed in the transition metal and Li layers, where white spheres correspond to octahedral cations (Li or Ni) in the Li layer. Such ordered arrangements can be described by a $a_{Mon.} \times a_{Mon.} \times c_{Mon.}$ monoclinic cell with space group $P2/m$, as shown in Figure 14a. The detailed crystallographic relationship between the parent and the $a_{Mon.} \times a_{Mon.} \times c_{Mon.}$ cells has been reported previously.[22] In the second model, we have empty and half partially occupied rows in both upper and lower tetrahedral sites, where octahedral cations and vacancies are randomly distributed in the transition metal and Li layers, as shown in Figure 14b. Such ordering can be described by a hexagonal $2a_{Hex.} \times 2a_{Hex.} \times c_{Hex.}$ supercell with space group $R\bar{3}m$. Similar long-range ordering in the octahedral sites of the Li layer can give rise to the appearance of these two superstructures, as shown in Figures 14c,d. Octahedral sites of two different occupancies (of Li and Ni) in the Li layer are ordered every other row, and octahedral cations and vacancies are randomly distributed in the transition metal layer, which can be described by the monoclinic $a_{Mon.} \times a_{Mon.} \times c_{Mon.}$ cell with space group $P2/m$. Alternate rows of partially occupied octahedral sites and vacancies are shown in Figure 14c. Similar configurations have been reported for ordering of one Li to one vacancy in $Li_{0.5}CoO_2$[22] and $Li_{0.5}NiO_2$.[23,38] In the fourth model, octahedral sites may be occupied partially every other row, and every other octahedral sites within each partially occupied row may be filled, where octahedral ions and vacancies are also randomly distributed in the transition metal layer. Such ordering of octahedral sites with two different occupancies in a ratio of 1:3 can be described by the hexagonal $2a_{Hex.} \times 2a_{Hex.} \times c_{Hex.}$ supercell with space group $R\bar{3}m$, as outlined in Figure 14d. This superstructure has been reported for $Li_{0.25}NiO_2$,[23] which consists of one Li to three vacancy ordering. The same supercell definition can also be used to describe three Li to one vacancy ordering in $Li_{0.75}NiO_2$.[23]

We use electron and X-ray diffraction simulation to examine different cation arrangements in these two supercells, identify unique diffraction features of each long-range cation ordering and compare these features with experimental diffraction data. One significant difference in the simulated electron diffraction patterns of these superstructures is the intensity of the doubling superlattice reflection arising from the $(104)_{Hex.}$ fundamental reflection relative to the other superlattice reflections, for a given occupancy of transition metal ions on the octahedral and tetrahedral sites. In case of

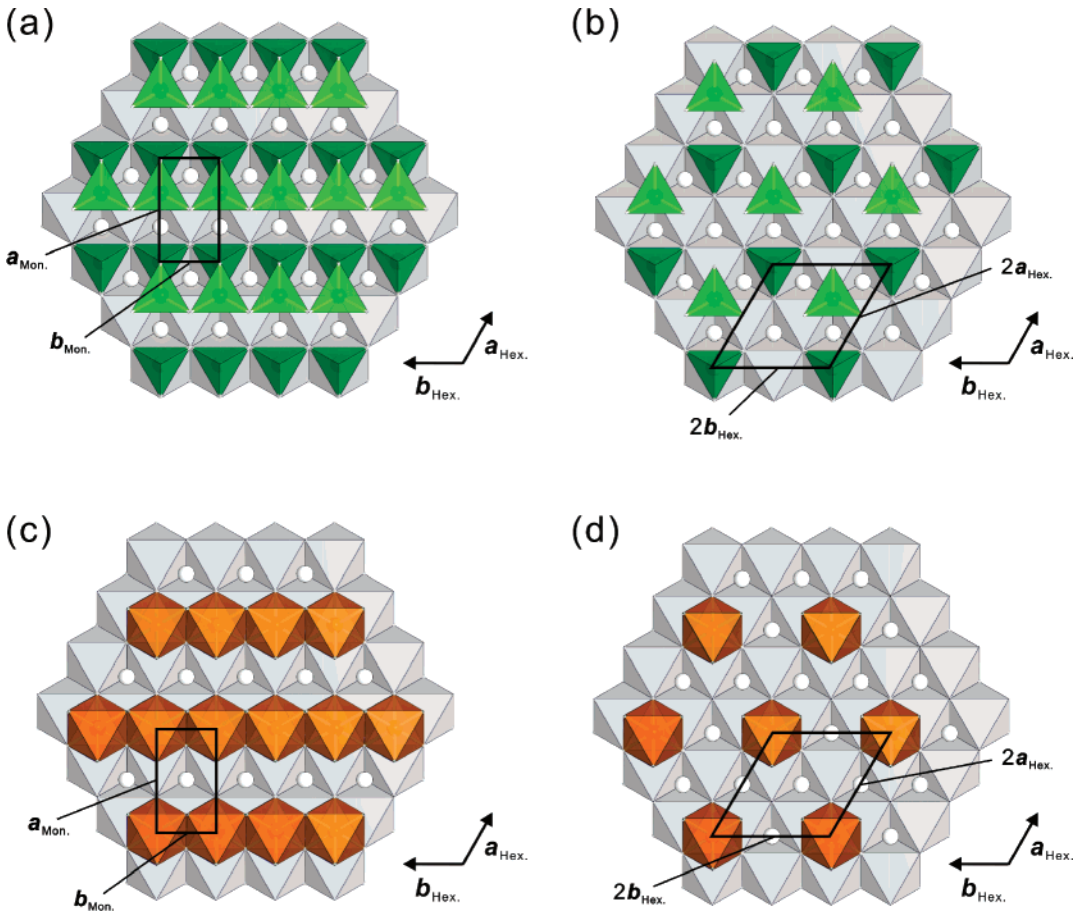

Figure 14. (a) Schematic of one ordered arrangement on the tetrahedral sites in the $a_{Mon.} \times a_{Mon.} \times c_{Mon.}$ supercell with space group $P2/m$. (b) Schematic of one ordered arrangement on the tetrahedral sites in the $2a_{Hex.} \times 2a_{Hex.} \times c_{Hex.}$ supercell with space group $R\bar{3}m$. (c) Schematic of one ordered arrangement on the octahedral sites in the $a_{Mon.} \times a_{Mon.} \times c_{Mon.}$ supercell with space group $P2/m$. (d) Schematic of one ordered arrangement on the octahedral sites in the $2a_{Hex.} \times 2a_{Hex.} \times c_{Hex.}$ supercell with space group $R\bar{3}m$.

tetrahedral ordering, the intensity of the $(104)_{Hex.}$ doubling superlattice reflections is zero if (1) cations and oxygen were located in the ideal positions of these tetrahedral sites (oxygen, 6c site $z = 1/4$, and cations, 6c site $z = 1/8$) and (2) the average occupancies of cations in the upper and lower tetrahedral sites were identical. Weak $(104)_{Hex.}$ doubling superlattice reflections might be found when these two above conditions are not met. On the other hand, ordering in the octahedral sites leads to strong $(104)_{Hex.}$ doubling superlattice reflections, which have the second strongest intensity among all superlattice reflections with the $(102)_{Hex.}$ reflections being the strongest. This difference can be visualized in the structural projections along the $(010)_{Hex.}$ direction. As shown in Figure 15a, ordering in the tetrahedral sites does not change the periodicity of the $(104)_{Hex.}$ planes and doubling of the $(104)_{Hex.}$ planes is not expected. On the other hand, tetrahedral ordering changes the periodicity of the $(108)_{Hex.}$ planes, which leads to the presence of doubling superlattice reflections in this reciprocal direction. In contrast, ordering in the octahedral sites changes the periodicity of the $(104)_{Hex.}$ and $(108)_{Hex.}$ planes, which can lead to the appearance of doubling superlattice reflections in both reciprocal directions, as shown in Figure 15b. This difference in the intensity of the $(104)_{Hex.}$ doubling superlattice reflections can be noted clearly in the simulated X-ray powder diffraction peak intensities of different tetrahedral and octahedral ordering configurations, as shown in Figure 15c. In the simulation, 0.06 Ni per formula unit were placed in the partially occupied tetrahedral sites of the Li layer (Figures 14a,b) or in the partially occupied octahedral sites in the Li layer (Figures 14c,d). As expected, random distributions of Ni and Li ions on the tetrahedral and octahedral sites do not lead to the appearance of any superlattice peaks, as shown by the two bottom patterns in Figure 15c. Although tetrahedral ordering leads to the appearance of many superlattice peaks similar to those of octahedral ordering, such as that of the $(108)_{Hex.}$ planes, the $(104)_{Hex.}$ doubling superlattice reflections is absent. In contrast, octahedral ordering in the $2a_{Hex.} \times 2a_{Hex.} \times c_{Hex.}$ supercell ($R\bar{3}m$) and the $a_{Mon.} \times a_{Mon.} \times c_{Mon.}$ supercell ($P2/m$) leads to strong $(104)_{Hex.}$ superlattice intensities relative to other superlattice peaks, as shown by the third and fifth patterns from the bottom in Figure 15c. Therefore, the appearance and the intensity of the $(104)_{Hex.}$ doubling superlattice reflection in the experimental electron diffraction patterns may be used to distinguish ordering on the octahedral and tetrahedral sites.

We now combine cation occupancies, simulated electron and X-ray data of different superstructural models, experimental electron diffraction results, and electrochemical measurements reported previously[12,27,42] to discuss likely ordering schemes in the charged and discharged samples.

Long-Range Ordering in the Charged Samples. We first focus on the 4.5 V charged $Li_{0.2}Ni_{0.5}Mn_{0.5}O_2$ sample. Although it had a relatively high fraction of crystals

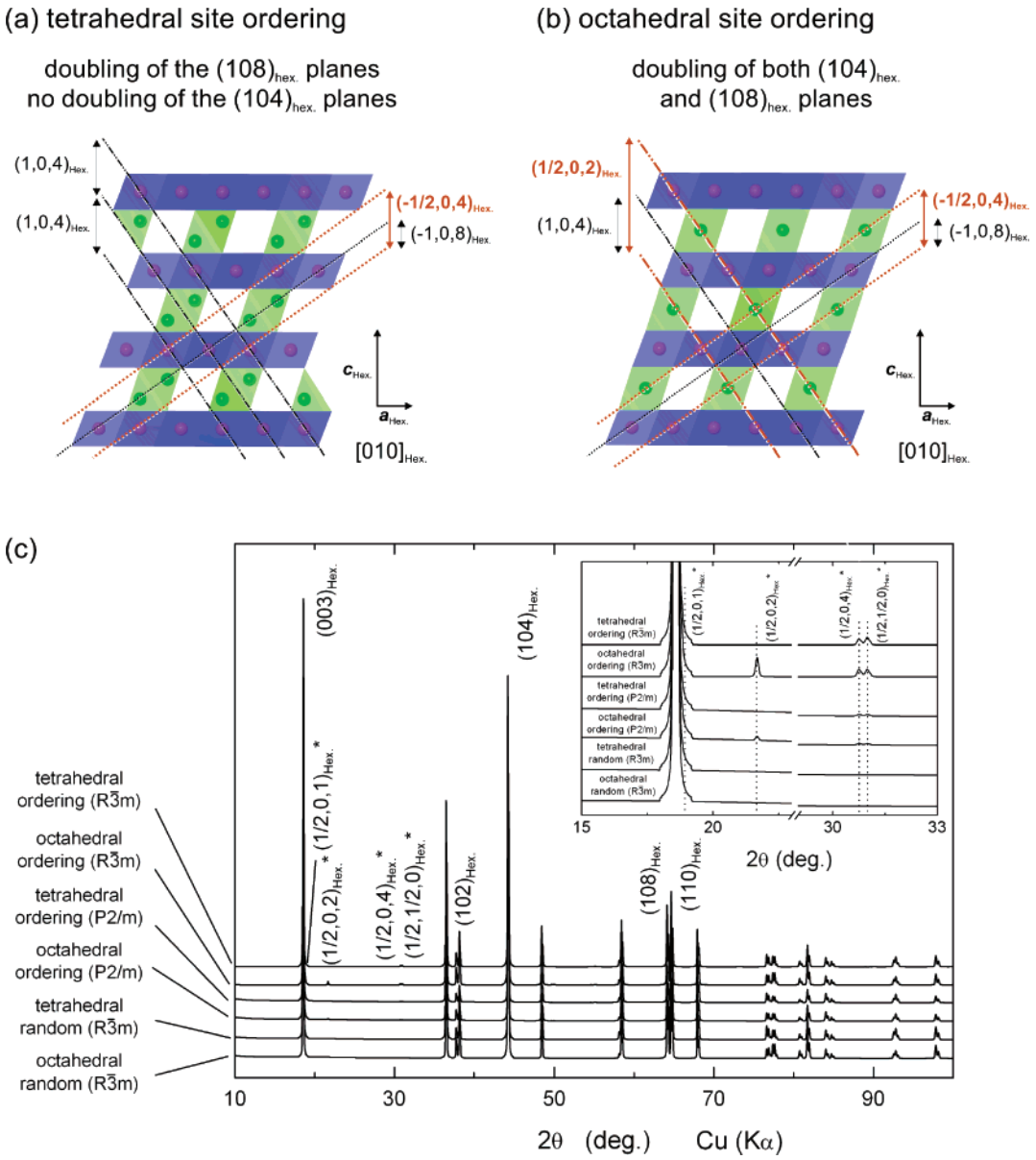

Figure 15. Schematic illustrations of $Li_xNi_{0.5}Mn_{0.5}O_2$ structure projected along the $[010]_{Hex.}$ zone axis for (a) tetrahedral ordering, where the $(104)_{Hex.}$ planes are not doubled and the $(108)_{Hex.}$ planes are doubled, and (b) octahedral ordering, where both sets of planes are doubled. (c) Simulated X-ray powder diffraction patterns of four superstructural models in Figure 14a,d and structures with a random distribution of tetrahedral or octahedral ions.

exhibiting superlattice reflections characteristic to the $a_{Mon.} \times a_{Mon.} \times c_{Mon.}$ or $2a_{Hex.} \times 2a_{Hex.} \times c_{Hex.}$ supercell, no superlattice peaks were found in the synchrotron X-ray powder diffraction data of this sample. This sample was shown to have 0.03 Ni per formula unit in the tetrahedral sites of the Li layer (Figure 11a), which is in good agreement with the work of Arachi et al. showing 0.02 Ni per formula unit in a $Li_{0.33}Ni_{0.5}Mn_{0.5}O_2$ electrode charged to 4.3 V.[12] In addition, it is believed that a considerable amount of Li ions may similarly exist in the tetrahedral sites of the Li layer in the 4.5 V charged sample as recent neutron diffraction studies reveal a considerable amount of tetrahedral Li ions (0.12 per formula unit) in the 4.6 V charged $Li_{0.33}Ni_{0.5}Mn_{0.5}O_2$ sample.[27] Moreover, 0.03 Ni per formula unit (Figure 11a) and presumably the remaining Li ions are located in the Li octahedral sites. Therefore, Ni (~0.03 per formula unit) and Li (~0.10 per formula unit) occupancies in the tetrahedral sites of the Li layer are similar to those of octahedral sites in the 4.5 V charged sample. Given the best distributions for long-range ordering in the tetrahedral and octahedral sites, octahedral ordering would lead to strong $(104)_{Hex.}$ superlattice reflections while tetrahedral ordering would lead to extremely weak or zero intensities for the $(104)_{Hex.}$ superlattice reflections. As the doubling superlattice reflections of the $(104)_{Hex.}$ planes were either absent (Figure 6b) or very weak (Figure 6a) relative to other superlattice reflections in the experimental patterns, it is proposed that these superlattice reflections found in the 4.5 V charged sample could be attributed primarily to ordering of Li, Ni, and vacancies in the tetrahedral sites of the Li layer.

Simulated patterns of tetrahedral ordering in the $a_{Mon.} \times a_{Mon.} \times c_{Mon.}$ and $2a_{Hex.} \times 2a_{Hex.} \times c_{Hex.}$ supercells along the equivalent zone axes of the experimental pattern in Figure 6a show that the doubling superlattice reflections of the $(104)_{Hex.}$ reflections are absent (see Supporting Information Figure S5a,b). In contrast, simulated electron diffraction

patterns of octahedral ordering in the $a_{Mon.} \times a_{Mon.} \times c_{Mon.}$ and $2a_{Hex.} \times 2a_{Hex.} \times c_{Hex.}$ supercells show the appearance of doubling superlattice reflections of the $(104)_{Hex.}$ type (see Supporting Information Figure S5c,d). In addition, it should be noted that the intensity of the $(104)_{Hex.}$ doubling superlattice reflections for octahedral ordering in the simulated X-ray powder diffraction patterns is strong relative to those of the other superlattice reflections (the third and the fifth patterns from the bottom in Figure 15c). As experimental electron diffraction observations in Figure 6a,b show zero or weak intensities for the $(104)_{Hex.}$ superlattice reflections, it is proposed that long-range ordering of Li, Ni, and vacancies in the tetrahedral sites of the Li layer may be more significant than octahedral ordering in the 4.5 V charged sample. As additional Li ions are removed from the structure and additional Ni ions migrate into the transition metal layer upon charging from 4.5 to 5.3 V, tetrahedral occupancies of Li and Ni in the Li and transition metal layers are reduced and thus tetrahedral ordering may become diminished. This argument is consistent with our observation that very few crystals examined from the 5.3 V sample show these doubling superlattice reflections (Figure 13).

Now we examine and discuss if the tetrahedral ordering can be better described by the $2a_{Hex.} \times 2a_{Hex.} \times c_{Hex.}$ ($R\bar{3}m$) or $a_{Mon.} \times a_{Mon.} \times c_{Mon.}$ supercell ($P2/m$) supercell. A number of experimental patterns exhibiting doubling superlattice reflections in the charged samples can be indexed consistently to both supercells. A few can be described uniquely by the $2a_{Hex.} \times 2a_{Hex.} \times c_{Hex.}$ ($R\bar{3}m$) supercell. For example, superlattice reflections of the $(10\bar{2})_{Hex.}$ and $(110)_{Hex.}$ planes are clearly visible but not the $(104)_{Hex.}$ ones in the $[241]_{Hex.}$ experiment pattern (Figure 7b), which can only be explained by the $2a_{Hex.} \times 2a_{Hex.} \times c_{Hex.}$ supercell ($R\bar{3}m$) but not the $a_{Mon.} \times a_{Mon.} \times c_{Mon.}$ supercell ($P2/m$). In the proposed $2a_{Hex.} \times 2a_{Hex.} \times c_{Hex.}$ ($R\bar{3}m$) superstructure (Figure 14b), no adjacent upper and lower tetrahedral sites are occupied (in contrast to the $a_{Mon.} \times a_{Mon.} \times c_{Mon.}$ supercell), which may minimize electrostatic repulsion among cations in the tetrahedral sites. In addition, partial occupancies of Ni and Li in the two different tetrahedral sites in Figure 14b might allow the superstructure to exist over a range of Li compositions. Therefore, it is hypothesized that tetrahedral ordering in the $2a_{Hex.} \times 2a_{Hex.} \times c_{Hex.}$ ($R\bar{3}m$) superstructure analogous to that shown in Figure 14b is most likely attributed to doubling superlattice reflections observed in the charged samples.

Long-Range Ordering in the Discharged Samples. The discharged samples have a large number of Li ions (~0.75−0.90 per formula unit) on the octahedral sites of the Li layer and a considerable amount of Ni ions (~0.06-~0.07 per formula unit) in the octahedral sites of the Li layer (Figure 11a).[27,42] In addition, small amounts of Ni (~0.01−0.02 Ni formula unit) may exist in the tetrahedral sites of the Li layer in the 4.5 V charged sample.[27,42] Moreover, it is believed that a considerable amount of Li ions may similarly exist in the tetrahedral sites of the Li layer in the 4.5 V charged sample as recent neutron diffraction studies reveal a considerable amount of tetrahedral Li ions (~0.04−0.19 per formula unit) in the discharged samples.[27] Therefore, Ni and Li occupancies on the octahedral sites of the Li layer are considerably greater than those in the tetrahedral sites of the Li layer in the discharged samples. It should be noted that Ni and Li occupancies in the tetrahedral sites in the discharged samples are similar to those found in the 4.5 V charged sample.

As synchrotron X-ray powder diffraction patterns of the 4.5 and 5.3 V discharged samples do not reveal any superlattice reflections, the extent of octahedral Ni (~0.06−0.07) ordering in the Li layer may not be significant in the long range. In addition, experimental electron diffraction patterns collected from the discharged samples did not exhibit strong superlattice reflections of the $(104)_{Hex.}$ planes. However, ordering of Li on the octahedral sites cannot be excluded, and it may occur in the discharged samples as a result of electrostatic forces among cations in-plane in the Li layer. Therefore, tetrahedral and octahedral ordering of Li, Ni, and vacancies may coexist in the layered structure and be responsible for the appearance of these superlattice reflections in the discharged samples.

As shown in Figure 9a, the presence of doubling superlattice reflections in the discharged samples can be better described by the $a_{Mon.} \times a_{Mon.} \times c_{Mon.}$ cell ($P2/m$) than the $2a_{Hex.} \times 2a_{Hex.} \times c_{Hex.}$ cell ($R\bar{3}m$). Such ordering may consist of alternate rows of fully and partially occupied octahedral Li and Ni and alternate rows of empty and partially occupied tetrahedral Li and Ni, as shown in Figure 9c. In addition, multiple orientation states of ordered domains may coexist in one crystal. Another $[\bar{2}\bar{4}\bar{1}]_{Hex.}$ zone axis pattern collected from the 4.5 V discharged samples is shown in Figure 9b, which can only be explained by considering two orientation states of ordered $a_{Mon.} \times a_{Mon.} \times c_{Mon.}$ domains in this crystal (Figure 9d). There are three independent orientation states (variants) of ordering in the $a_{Mon.} \times a_{Mon.} \times c_{Mon.}$ cell having space group $P2/m$ with respect to the parent cell with rhombohedral symmetry ($R\bar{3}m$). Ordering in different orientation states may occur within one $Li_xNi_{0.5}Mn_{0.5}O_2$ crystal during electrochemical cycling, and these variants may exist within one Li layer and/or in different Li layers. Similar microstructures have been reported previously in layered Li_xCoO_2[22,45,46] and Li_xNiO_2[23] compounds.

Conclusions

Single-crystal electron diffraction analyses of pristine and cycled $Li_xNi_{0.5}Mn_{0.5}O_2$ samples have shown that the fraction of crystals exhibiting the $\sqrt{3}a_{Hex.} \times \sqrt{3}a_{Hex.} \times c_{Hex.}$ superlattice reflections significantly decreases upon charging to 4.5 and 5.3 V. The disappearance and weakening of the $\sqrt{3}a_{Hex.} \times \sqrt{3}a_{Hex.} \times c_{Hex.}$ superlattice reflections can be explained by Ni migration from the Li to the transition metal layer and increasing Ni occupancy in the transition metal layer upon charging to high voltages, which is in good agreement with previous powder diffraction studies.[27,42] The process of Ni migration occurs over a wide range of charging voltage as the extent would be dependent on the oxidation

(45) Chiang, Y. M.; Wang, H. F.; Jang, Y. I. *Chem. Mater.* **2001**, *13*, 53.
(46) Shao-Horn, Y.; Weill, F.; Croguennec, L.; Carlier, D.; Menetrier, M.; Delmas, C. *Chem. Mater.* **2003**, *15*, 2977.

state of Ni ions and Li content and the local environments of Ni ions in the Li layer. Although the onset voltage of Ni migration and the corresponding Li content of the sample cannot be determined in this study, a considerable change in the Ni occupancy of the transition metal layer has been found in the $Li_{0.2}Ni_{0.5}Mn_{0.5}O_2$ sample charged to 4.5 V. In addition, some crystals of $Li_xNi_{0.5}Mn_{0.5}O_2$ electrodes charged to 5.3 V have transformed from the O3 to the O1 (CdI_2) structure, indicating that nearly all the nickel ions may be removed from the Li layer of $Li_xNi_{0.5}Mn_{0.5}O_2$, similar to Li_xCoO_2 and Li_xNiO_2.

Although Ni migration is shown to be partly reversible upon discharge, the discharged samples have considerably lower amounts of cation disorder or interlayer mixing of Li and Ni in comparison to the pristine sample. It is believed that the excellent reversibility of $LiNi_{0.5}Mn_{0.5}O_2$, even with a considerable amount of cation disorder (~0.10 per formula unit), could be attributed to the mobility and migration of Ni ions in the layered structure upon Li removal, which can facilitate Li diffusion in the Li slab space. Furthermore, exposing $Li_xNi_{0.5}Mn_{0.5}O_2$ electrodes to 5.3 V can increase the fraction of Ni ions that permanently remain in the transition metal layer with respect to cycling to 4.5 V only, which is in good agreement with improved rate capability of electrodes exposed to 5.3 V.[42] The improved stability of Ni ions in the transition metal layer in the 5.3 V charged sample might be argued from the structural perspective: the reduction in the Li interslab space and/or the formation of the O1 structure makes Ni hopping out of the octahedral sites in the transition metal layer into adjacent, face-shared tetrahedral sites in the Li layer more difficult than the O3 structure of the 4.5 V charged sample upon reduction to Ni^{2+} during initial discharge.

Electron diffraction data have shown additional superlattice reflections in a subset of crystals from the cycled samples, which are indicative of new long-range cation ordering in a $2a_{Hex.} \times 2a_{Hex.} \times c_{Hex.}$ supercell with space group $R\bar{3}m$ and/or an $a_{Mon.} \times a_{Mon.} \times c_{Mon.}$ supercell having space group $P2/m$. The exact physical nature of these superlattice reflections is not understood fully. It is proposed from electron diffraction evidence that ordering of Li, Ni, and vacancies occurs in the tetrahedral sites of the Li layer with partial occupancy in the $2a_{Hex.} \times 2a_{Hex.} \times c_{Hex.}$ supercell in the charged samples. Such an ordering configuration in the tetrahedral sites may minimize electrostatic interactions among cations and stabilize the O3 structure upon charging to high voltages. On the other hand, it is proposed that long-range ordering of Li, Ni, and vacancies in the tetrahedral sites of the Li layer and long-range ordering of Li and vacancies may coexist in some crystals of the discharged samples that can be described by the $a_{Mon.} \times a_{Mon.} \times c_{Mon.}$ cell with space group $P2/m$. Partial occupancy of Li and Ni ions on the tetrahedral and octahedral sites can allow the proposed superstructures to be accommodated and exist over a range of Li compositions.

These superstructures proposed for the charged and discharged $Li_xNi_{0.5}Mn_{0.5}O_2$ samples based on electron diffraction data were not detected in the synchrotron X-ray powder diffraction data nor in the differential capacity plots of $Li/Li_xNi_{0.5}Mn_{0.5}O_2$ cells. This is because not only is electron diffraction more sensitive to ordering of light atoms and partial occupancy of heavy atoms than X-rays, but also single-crystal electron diffraction analysis can better detect ordered minor phases than X-ray powder diffraction and electrochemical data that provide average information over the entire sample. It should be also mentioned that based on the electron diffraction evidence presented here, we cannot exclude long-range ordering configurations other than the ones described in this manuscript nor short-range ordering of Li, Ni, and vacancies in these materials.

Acknowledgment. The authors would like to acknowledge Y.-T. Kim for collecting synchrotron X-ray diffraction data of cycled samples and G. Ceder for fruitful discussions. This work is supported in part by the Office of Naval Research Young Investigator Award N00014-03-10448, the MRSEC Program of the National Science Foundation under award number DMR 02-13282, a MIT Presidential Fellowship, and the Assistant Secretary for Energy Efficiency and Renewable Energy, Office of FreedomCAR and Vehicle Technologies, of the U.S. Department of Energy under Contract No. DE-AC03-76SF00098 via Subcontract Nos. 6517749 and 6804921 with the Lawrence Berkeley National Laboratory. Figures 2, 3, 8, 9, 14, and 15 were drawn with VICS-II software developed by K. Momma and F. Izumi.

Supporting Information Available: Simulated electron diffraction patterns (PDF). This material is available free of charge via the Internet at http://pubs.acs.org.

CM070139+